Effects of subcritical and supercritical CO_2 sorption on deformation and failure of high-rank coals

Renato Zagorščak[a]* and Hywel Rhys Thomas[a]

[a] Geoenvironmental Research Centre (GRC), School of Engineering, Cardiff University, The Queen's Buildings, The Parade, Cardiff, CF24 3AA

*corresponding author (ZagorscakR@cardiff.ac.uk)

Abstract:

This paper presents the results of an extensive experimental analysis aimed at establishing the effects of subcritical and supercritical CO_2 sorption on deformation and failure of coals. Two high-rank anthracitic coals from the South Wales coalfield, obtained from different locations and depths of 150 m and 550 m, are employed for that purpose. The investigations include i) determination of unconfined compressive strengths and elastic moduli of the cores both non-saturated and saturated with CO_2 at 2.1 MPa, 4.3 MPa and 8.5 MPa, ii) assessing the dependence of the parameters obtained on CO_2 pressure, iii) analysing the effect of CO_2 saturation on failure patterns of the samples tested and iv) determination of the particle size distribution after the failure of the samples. Based on the results of twenty coal specimens tested, it is demonstrated that CO_2 sorption reduces the uniaxial compressive strengths and elastic moduli by between 29% and 83% for the range of pressures studied. The reductions observed increase gradually up to 4.3 MPa and then reach a plateau. By accommodating the effect of effective stress on compressive strength values, it is shown that chemical weakening of high rank coals is mostly associated with sorption of subcritical CO_2, with negligible impact of supercritical CO_2 on further parameter reduction. Inspection of failure patterns during uniaxial compression suggests that non-saturated coal specimens fail through axial splitting with rapid crack propagation and high outburst of coal pieces while the failure of cores subjected to CO_2 injection occurs through multiple fractures with negligible material outburst. The post-failure analysis demonstrates that CO_2 treated samples disintegrate on smaller particles than non-saturated specimens, as up to 5.6 more CO_2 saturated coal pieces passed through the sieves considered in this study than non-saturated pieces. It is claimed that this study presents novel insights into the geomechanical response of high rank anthracitic coals to high pressure CO_2 injection.

Keywords: Coal, Carbon sequestration, Geomechanics, Strength, Elastic modulus, CO_2 adsorption

1. Introduction

Geological sequestration in unmined coal seams offers a prospect of delivering greenhouse gas emissions reductions and at the same time offsetting the costs of CO_2 capture, transportation and storage as the injection of CO_2 in the coal beds allows the production of a value-added product such as methane (White et al., 2005). In general, numerous studies have shown that coal can hold at least twice the volume of CO_2 as CH_4 (Jones et al., 2004; White et al., 2005). However, coals are a mixture of inorganic minerals and organic material that may be affected during the gas injection and adsorption process (Karacan, 2007; Gathitu et al., 2009). Hence, understanding the response of coal under applied stress and storage conditions is of importance for the integrity and safety of the coal seams targeted for CO_2 sequestration and the overlaying strata. This paper aims to enhance such understanding by presenting the experimental investigation of the effects of sub-critical and supercritical carbon dioxide saturation on high-rank coal failure and elastic deformation under uniaxial compressive stress conditions.

The most favourable coal seams for sequestration are occurring at depths where pressure and temperature may exceed the critical values of CO_2, i.e. 750 m (White et al., 2005). At such depths, high rank coals offer a great prospect of storing CO_2 as the maximum sorption capacity generally increases with coal rank (Li et al., 2011; Busch and Gensterblum, 2010). This is related to the fact that high rank coals predominantly contain micropores which provide most of the surface area where gas can adsorb (White et al., 2005).

To date, most research efforts were focused in investigating the geomechanical behaviour of lignite and bituminous coals predominantly exposed to CO_2 in the sub-critical state (Viete and Ranjith, 2006; Perera et al., 2011; Ranjith ad Perera, 2012; Perera, 2013; Perera et al., 2013; Hol et al., 2014; Masoudian et al., 2014; Vishal et al., 2015; Ranathunga et al., 2016a; 2016b). Several studies indicated that CO_2 saturation and induced swelling cause crack initiation and enhancement of the fracture lines along the coal increasing the total pore volume (Larsen, 2004; Liu et al., 2010; Hol et al., 2012; Liu et al., 2015). However, very little is known about how anthracitic coals respond to compression after being treated with CO_2, in particular in the supercritical state.

Hence, the geomechanical response of high-rank anthracitic coals under a range of both subcritical and supercritical CO_2 injection pressures up to 8.5 MPa is investigated and discussed in this paper. The results of uniaxial compressive tests of two sets of coal samples obtained from different depths and locations in the South Wales Coalfield are presented. In total, eight samples are tested in natural air-dried state without CO_2 saturation. Twelve specimens were exposed to different sub-critical and supercritical CO_2 pressures for two weeks before testing. Based on the stress-strain data obtained, unconfined compressive strengths and elastic moduli are calculated and presented. In addition, the change in the measured parameters with an increase in gas saturation pressure is shown and discussed. The reductions in elastic moduli and unconfined compressive strengths are quantified by applying a fitting curve to the experimentally determined values and obtaining the parameters related to the reduction of deformation properties as a function of gas pressure. Failure patterns of non-saturated and CO_2 saturated specimens of both coals are analysed and discussed, based on the photographs taken before and after the coal failure. The distribution of particle sizes after the failure of the samples is also examined.

2. Methodology

2.1. Samples

Coal blocks were collected from two different coal mines, the East Pit East Opencast Coal Site and the Aberpergwm drift coal mine from depths of 150 m and 550 m, respectively. Both coal mines are located in Wales as a part of the South Wales Coalfield (Fig. 1). Coal extracted from the East Pit East Opencast Coal Site is locally known as Black Diamond while coal from the Aberpergwm mine is from a 9ft seam layer and in the future text they will be referred as BD and AB, respectively. The coal blocks obtained on site were wrapped in cling film and put in plastic bags to minimize the oxidation of the coal surfaces and preserve chemical and physical properties. Upon arrival in the laboratory, the sealed blocks were labelled and stored in the constant room temperature environment.

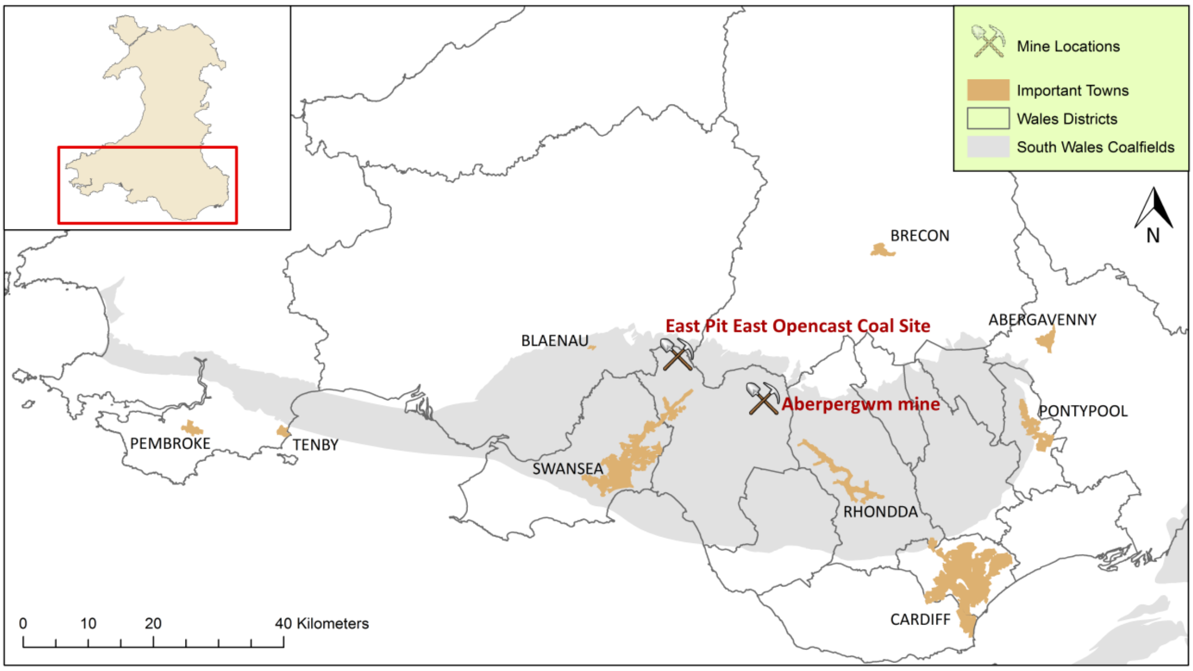

Fig. 1. South Wales Coalfield and locations of the East Pit East Opencast Coal site and the Aberpergwm drift mine.

Coal cores were drilled out of the coal blocks using a coring machine. Water was used as a cooling agent while drilling. Diamond core drilling bit with an internal diameter of 36 mm was used to obtain the coal cores from the Black Diamond and 9ft seam blocks (Fig. 2). Preparation of coal samples for the experiments was conducted following the ASTM D2013/D2013M (2012) standard of practice. As the drying of coal at temperatures higher than 70°C might create new cracks and small fissures leading to alteration of the physical structure of coal (e.g. Gathitu et al., 2009), an air-drying method following the ASTM D3302/D3302M (2015) was applied.

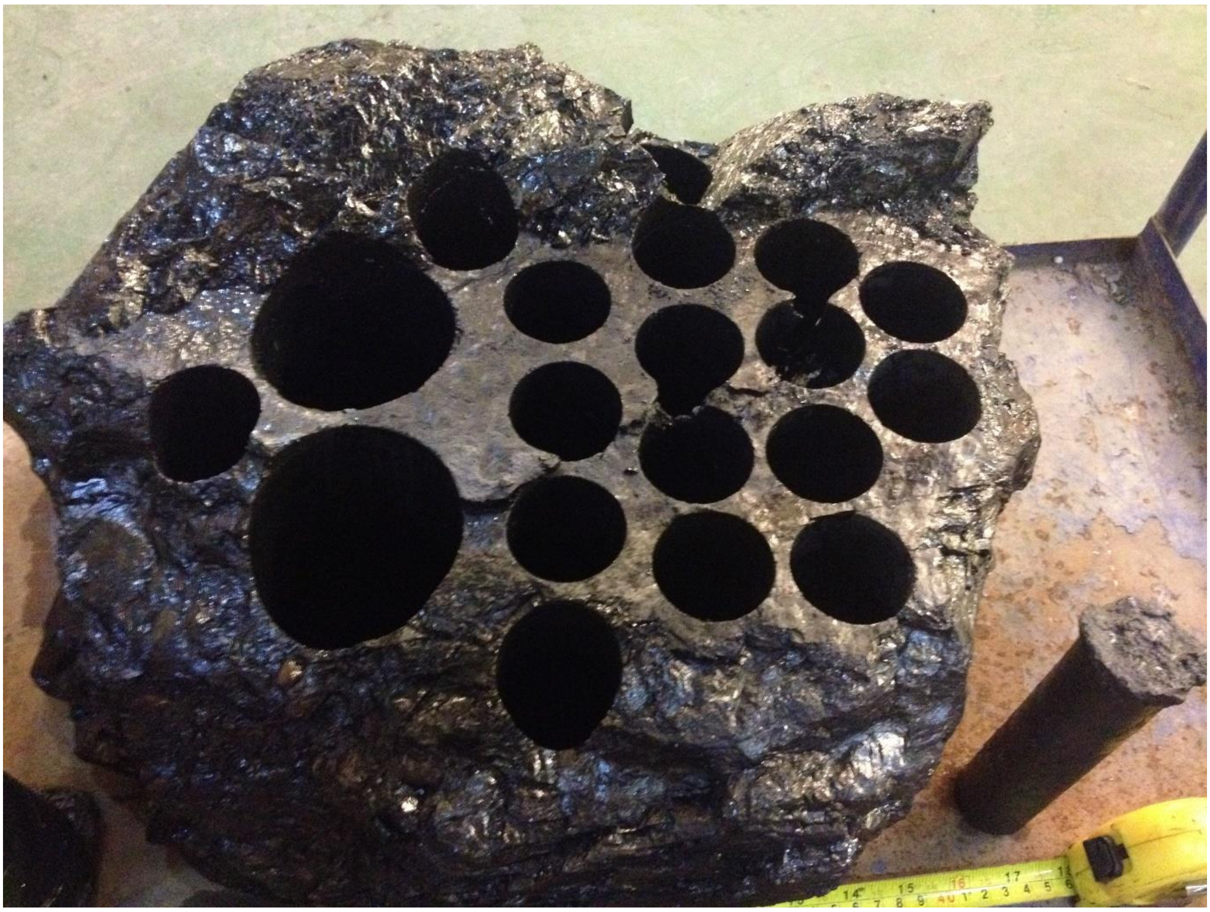

Fig. 2. A typical coal block used for the extraction of coal samples for uniaxial compressive tests.

A total of twenty coal cores were selected for the uniaxial compressive testing. Although a larger number of coal cores has been extracted, only the ones with minimum fractures or small inconsistencies were chosen. The dimensions of the selected samples are shown in Table 1 together with the measured values of mass and density for each core. The average densities of both BD and AB samples are the same, i.e. 1376 kg/m^3.

Crushed samples passed through a sieve size of 0.212 mm were used for the Proximate and Ultimate analyses, and the results are presented in Table 2. Proximate analysis was performed in accordance to British Standard (BS 1016-104.3, 1998; BS 1016-104.4, 1998; BS 1016-104.1, 1999), while the Ultimate analysis was conducted following the BS 1016-106.1.1 (1996) and BS 1016-106.4.2 (1996). Both BD and AB coals contain high percentage of fixed carbon content, i.e. 90.9% and 88.7%, respectively. Moisture contents, ash contents and volatile matter contents for both samples are relatively low, i.e. 1.65%, 1.65%, 5.82% for BD coal and 0.91%, 4.62%, 5.73% for AB coal, respectively. Based on the results obtained and the comparison with the ASTM D388 (2015) classification of coal rank, both BD and AB coals can be classified as high rank anthracitic coals.

Table 1
Dimensions and physical properties of core samples used in the uniaxial compressive tests.

Sample	Diameter (cm)	Length (cm)	L/D ratio	Mass (g)	Density (g/cm^3)
Black Diamond					
BD1	3.6	7.6	2.1	107.4	1.376
BD2	3.6	7.6	2.1	107.5	1.376
BD3	3.6	7.7	2.1	108.4	1.373
BD4	3.6	7.6	2.1	108.3	1.378
BD5	3.6	7.5	2.1	106.5	1.377
BD6	3.6	7.5	2.1	106.2	1.377
BD7	3.6	7.3	2.0	103.1	1.374
BD8	3.6	7.1	2.0	101.0	1.378
BD9	3.6	7.4	2.1	104.6	1.370
BD10	3.6	7.2	2.0	101.7	1.380
Average	**3.6**	**7.5**	**2.1**	**105.4**	**1.376±0.003**
9ft Aberpergwm					
AB1	3.6	7.5	2.1	108.3	1.391
AB2	3.6	6.9	1.9	98.5	1.376
AB3	3.6	6.8	1.9	96.5	1.376
AB4	3.6	7.9	2.2	113.3	1.389
AB5	3.6	5.6	1.6	78.9	1.367
AB6	3.6	5.6	1.6	80.2	1.392
AB7	3.6	6.0	1.7	83.9	1.364
AB8	3.6	6.4	1.8	89.4	1.365
AB9	3.6	5.3	1.5	74.7	1.365
AB10	3.6	7.5	2.1	106.7	1.379
Average	**3.6**	**6.6**	**1.8**	**93.0**	**1.376±0.011**

Table 2
Results of the Proximate and Ultimate Analyses.

Characterization test	Black Diamond	9ft Seam
Proximate analysis		
Moisture content, %	1.65±0.12	0.91±0.3
Ash content, %	1.65±0.38	4.62±0.3
Volatile matter, %	5.82±0.21	5.73±0.08
Fixed carbon content, %	90.88	88.73
Ultimate analysis		
Total carbon content, %	90.12±0.11	89.5±0.66
Total sulphur content, %	0.95±0.02	0.87±0.04

2.2. Experimental procedure

In total, twenty coal specimens were tested via an unconfined uniaxial compressive test. Four natural (non-saturated) specimens from each coal seam (BD and AB) were analysed without CO_2 saturation. Six specimens from each coal seam were saturated with CO_2 at designated pressures before uniaxial compression.

Saturation of samples with carbon dioxide was performed in a manometric sorption cell, manufactured by GDS Instruments, which has been used as a saturation chamber for this purpose (Fig. 3). The cell can tolerate pressures up to 20 MPa and temperatures up to 338K. The adsorption cell contains two cavities, each with a volume of approximately 150 cm^3. Each chamber is fitted with a GDS Instruments pressure transducer measuring up to 32 MPa and with an accuracy of 0.15%. The cell was placed in a stainless steel tank filled with deionised water which was heated to the designated temperature using Thermo Haake temperature controller with an accuracy of ±0.01K. A high pressure injection unit consisting of a dual syringe Teledyne Isco 500D pump system was employed to pressurize CO_2 to the required experimental pressures. The capacity of each syringe pump is 507.38 mL with a pressure range between 0.07 – 25.9 MPa and a standard pressure accuracy of 0.5%. Constant temperature of the pumps was achieved using a Huber Pilot One Ministat 125 temperature controller which circulates deionised water contained in the 2.75 L water tank through heating jackets. Syringe pumps were connected to a liquid withdrawal carbon dioxide cylinder with 99.99% purity in which the tube runs down the centre of the pressurised cylinder and draws the liquid up through the valve. Due to possible contaminants within the cylinder, a filter was fitted at the top of the cylinder. Before injecting CO_2, samples and the pipeline had been vacuumed for one hour to remove any trapped air. Buchi vacuum pump with a pressure of -0.09 MPa was used for that purpose. After that, CO_2 was injected at a designated pressure and kept constant for two weeks. The saturation time of two weeks was based on the work of Zagorščak (2017) who demonstrated that this is sufficient time for the CO_2 to adsorb on the intact specimens of the high-rank coals.

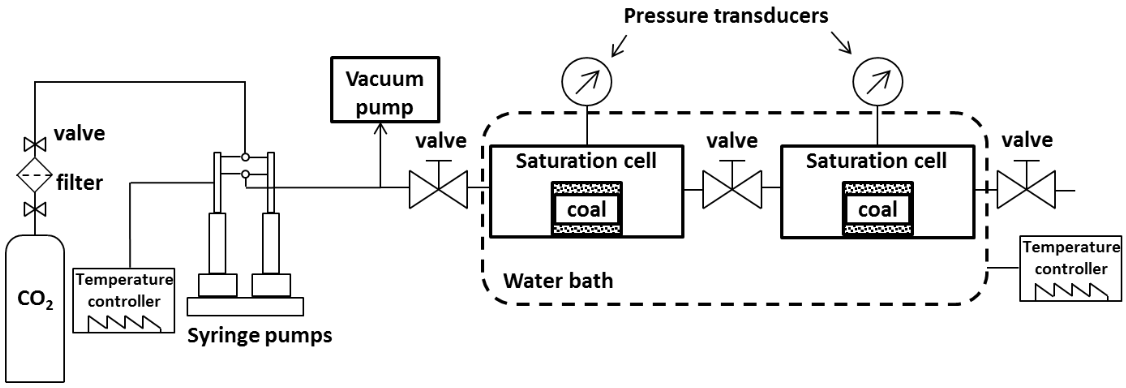

Fig. 3. Schematic of the system used for CO_2 saturation of the samples.

Upon the completion of saturation, chambers were slowly depressurized to avoid any sudden change in pressure which could damage the samples. After removing the specimens from the saturation chamber, they were wrapped in a plastic cling film and tested within a maximum time of one hour.

Uniaxial compressive tests were performed using a Shimadzu Autograph Load Cell AG-I with maximum load capacity of 20 kN. Specimens were placed between top and bottom steel platens. To minimize the impact of a potential unevenness of the sample surface on measured results, two steel blocks were placed between the sample and the top platen. Blocks were able to move with respect to each other when facing uneven surface allowing equal distribution of stress on the coal specimen. Upon sample placement, the axial load on the specimen was then increased and measured continuously.

An attached smart controller showed test force and displacement in real-time, allowing fine position adjustment. Specimens were subjected to a constant loading rate of 0.1 mm/min where the axial displacement of the samples was recorded simultaneously using the built-in displacement transducer of the loading machine. Both the uniaxial compressive strength (UCS) and elastic modulus (E) were calculated following the ASTM D7012 (2014).

2.3. Experimental conditions

Table 3 summarizes the number of specimens and saturation conditions. Results obtained on natural (non-saturated) specimens represent a baseline for all other tests carried out on samples saturated with CO_2 under different saturation conditions.

Table 3
Saturation pressures applied to the coal samples.

Samples	Saturation pressures (MPa) 1st step ~2.1 MPa	2nd step ~4.3 MPa	3rd step ~8.5 MPa
Black Diamond			
BD1, BD2, BD3, BD4		No saturation	
BD5	2.12	-	-
BD6	2.12	-	-
BD7	-	4.32	-
BD8	-	4.35	-
BD9	-	-	8.56
BD10	-	-	8.55
9ft Aberpergwm			
AB1, AB2, AB3, AB4		No saturation	
AB5	2.05	-	-
AB6	2.05	-	-
AB7	-	4.25	-
AB8	-	4.25	-
AB9	-	-	8.46
AB10	-	-	8.46

Due to the fact that transition from subcritical to supercritical CO_2 can cause changes in the sorptive potential of CO_2 affecting coal's behaviour (e.g. Perera et al., 2013), temperature of the manometric sorption system was maintained at 313±0.01K (40±0.01°C) enabling carbon dioxide to achieve its supercritical state at high pressures. It should be noted that pressure values mentioned in this study are absolute pressure values calculated assuming the atmospheric pressure of 101 325 Pa. If an average hydrostatic gradient of 0.01 MPa/m and an average thermal gradient of 0.03 K/m (°C/m) with an average surface temperature of 285K (12°C) are assumed (e.g. Gensterblum, 2013), results of this study represent conditions existing up to approximately 900 m of depth.

2.4. Sieve Analysis

In order to get further insights into the post-failure particle size distribution, Black Diamond specimens were analysed immediately after the failure, i.e. four non-saturated specimens and six CO_2 saturated specimens. Sieves with openings of 6.3 mm, 4 mm, 2 mm, 1.18 mm, 0.6 mm and 0.425 mm were used. Calculation of the mass passing through a certain sieve followed a procedure stated in BS 1337-2 (1990).

3. Experimental results and analysis

Axial stress versus strain curves for non-saturated and CO_2 saturated specimens from Black Diamond and 9ft Aberpergwm coal seams are presented in Fig. 4 and Fig. 5, respectively. By comparing the figures, it can be observed that the stress-strain behaviour of the samples saturated with CO_2 is different than of non-saturated samples. In particular, the samples exposed to CO_2 can be compressed more for the same value of applied stress than the non-saturated samples.

Slopes of the curves and maximum recorded stress values of 10 MPa obtained on non-saturated BD specimens are comparable (Fig. 4). The exception is sample BD3 which experienced failure at a lower value of applied stress, i.e. 8 MPa. Fig. 5 shows that the slopes of the curves of non-saturated AB specimens are also comparable, however; maximum recorded stress values range between 5.9 MPa and 9.1 MPa.

Experimental results of the two BD specimens saturated with CO_2 at 2.1 MPa show comparable behaviour with maximum recorded stress values of 6.3 MPa (Fig. 4). Although both AB specimens saturated at 2.1 MPa show similar slopes of the curves, maximum stress values are 3.6 MPa and 4.6 MPa (Fig. 5).

Two BD specimens saturated at 4.3 MPa and two saturated at 8.5 MPa show peak stress values of 2.3 MPa and 1.7 MPa, and 2.9 MPa and 2.4 MPa, respectively (Fig. 4). Similarly, AB samples saturated at 4.3 MPa show maximum stress values of 1.3 MPa and 1.9 MPa, while samples saturated at 8.5 MPa show maximum stresses of 1.5 MPa and 2.1 MPa (Fig. 5).

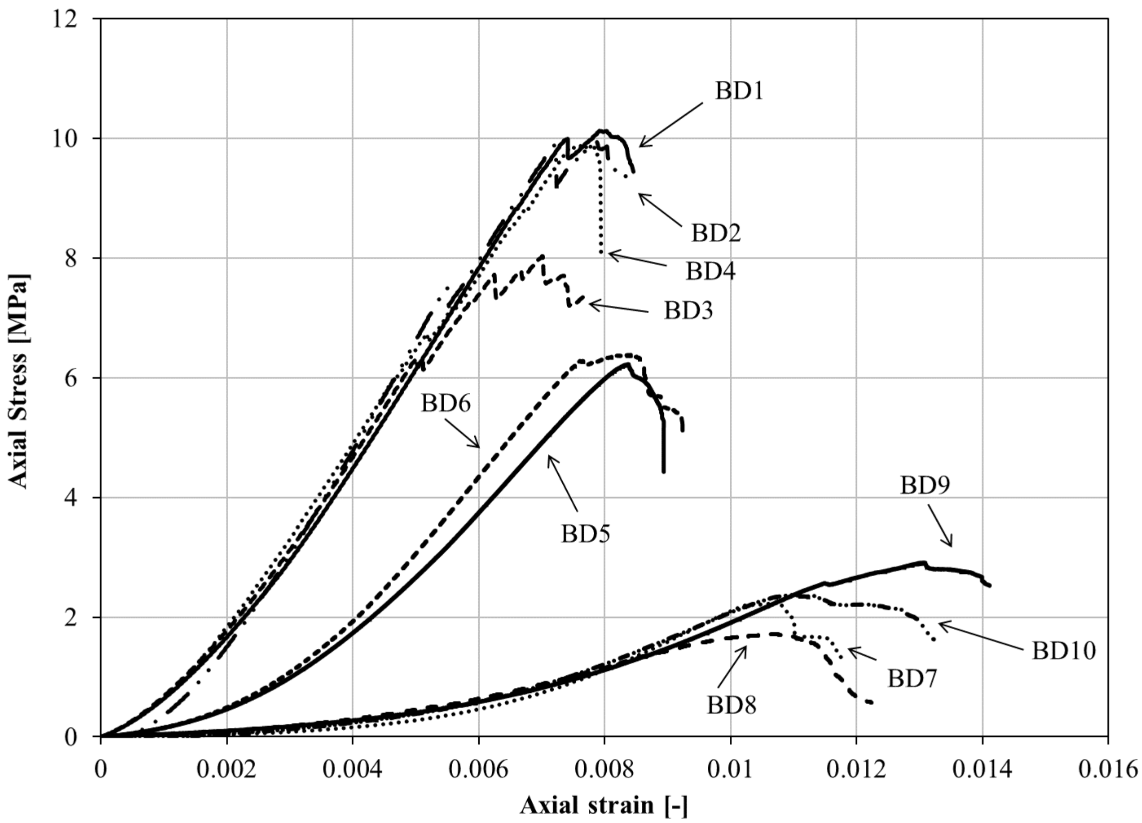

Fig. 4. Axial stress versus strain curves of natural and CO_2-saturated Black Diamond specimens.

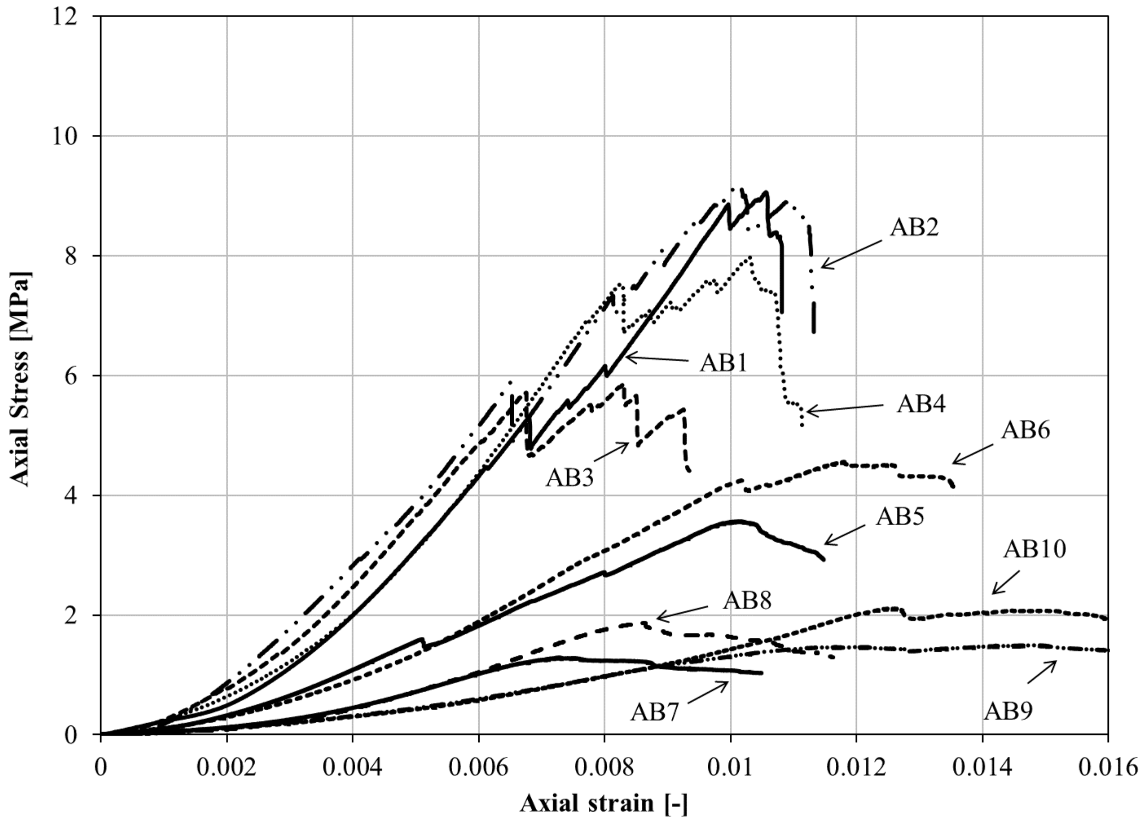

Fig. 5. Axial stress versus strain curves of natural and CO_2-saturated 9ft Aberpergwm specimens.

Calculated values of elastic moduli and unconfined compressive strengths of BD and AB samples are presented in Table 4. Based on the unconfined compressive strengths and elastic moduli of non-saturated specimens and samples saturated at different pressures of each coal, average values are also calculated and presented. In addition, reductions of average values of CO_2-saturated samples with respect to the average values of non-saturated samples are shown.

The relationship between the average elastic modulus of non-saturated samples and CO_2-saturated samples used to calculate the reductions presented in Table 4 is:

$$\Delta E = \left(1 - \frac{E_{CO_2}}{E_{natural}}\right) \times 100 \quad (1)$$

where ΔE is the reduction in elastic modulus, $E_{natural}$ (GPa) and E_{CO_2} (GPa) are the elastic moduli of natural (non-saturated) and CO_2-saturated specimens, respectively.

Similarly, reduction in unconfined compressive strength (ΔUCS) is expressed as:

$$\Delta UCS = \left(1 - \frac{UCS_{CO_2}}{UCS_{natural}}\right) \times 100 \quad (2)$$

where $UCS_{natural}$ (MPa) and UCS_{CO_2} (MPa) are the unconfined compressive strengths of natural (non-saturated) and CO_2-saturated samples, respectively.

Table 4.
Unconfined compressive strengths and elastic moduli of natural (non-saturated) and CO_2-saturated Black Diamond and 9ft Aberpergwm coal samples.

Specimen	L/D ratio	UCS (MPa)	Average UCS (MPa)	ΔUCS (%)	E (GPa)	Average E (GPa)	ΔE (%)
Black Diamond							
Natural (non-saturated)							
BD1	2.1	10.12			1.51		
BD2	2.1	9.97	9.51	-	1.72	1.59	-
BD3	2.1	8.03	±0.86		1.53	±0.08	
BD4	2.1	9.90			1.57		
2.1 MPa saturated							
BD5	2.1	6.23	6.31	-33.7	1.04	1.13	-29.0
BD6	2.1	6.38	±0.08		1.21	±0.08	
4.3 MPa saturated							
BD7	2.0	2.26	1.99	-79.1	0.48	0.37	-76.8
BD8	2.0	1.72	±0.27		0.26	±0.11	
8.5 MPa saturated							
BD9	2.1	2.91	2.65	-72.2	0.39	0.40	-74.8
BD10	2.0	2.38	±0.27		0.42	±0.02	

9ft Aberpergwm							
Natural (non-saturated)							
AB1	2.1	9.06	8.01 ±1.33	-	1.15	1.13 ±0.04	-
AB2	1.9	9.15			1.06		
AB3	1.9	5.86			1.15		
AB4	2.2	7.97			1.16		
2.1 MPa saturated							
AB5	1.6	3.57	4.06	-49.3	0.41	0.49	-56.3
AB6	1.6	4.56	±0.49		0.58	±0.08	
4.3 MPa saturated							
AB7	1.6	1.29	1.58	-80.3	0.28	0.29	-74.5
AB8	1.8	1.87	±0.29		0.30	±0.01	
8.5 MPa saturated							
AB9	1.5	1.50	1.80	-77.5	0.18	0.19	-82.9
AB10	2.1	2.11	±0.31		0.21	±0.02	

It can be seen from Table 4 that the average elastic moduli of non-saturated BD and AB specimens are 1.59 GPa and 1.13 GPa, respectively. BD specimens saturated with CO_2 at 2.1 MPa, 4.3 MPa and 8.5 MPa exhibit the average elastic moduli of 1.13 GPa, 0.37 GPa and 0.4 GPa, respectively. The average elastic moduli of AB specimens saturated with CO_2 at 2.1 MPa, 4.3 MPa and 8.5 MPa pressures are 0.49 GPa, 0.29 GPa and 0.19 GPa, respectively.

In order to establish a relationship between the measured parameters of all samples, unconfined compressive strengths versus elastic moduli of all tested specimens are plotted in Fig. 6. Elastic modulus and unconfined compressive strength show linear relationship, i.e. samples with higher strength show higher values of elastic modulus.

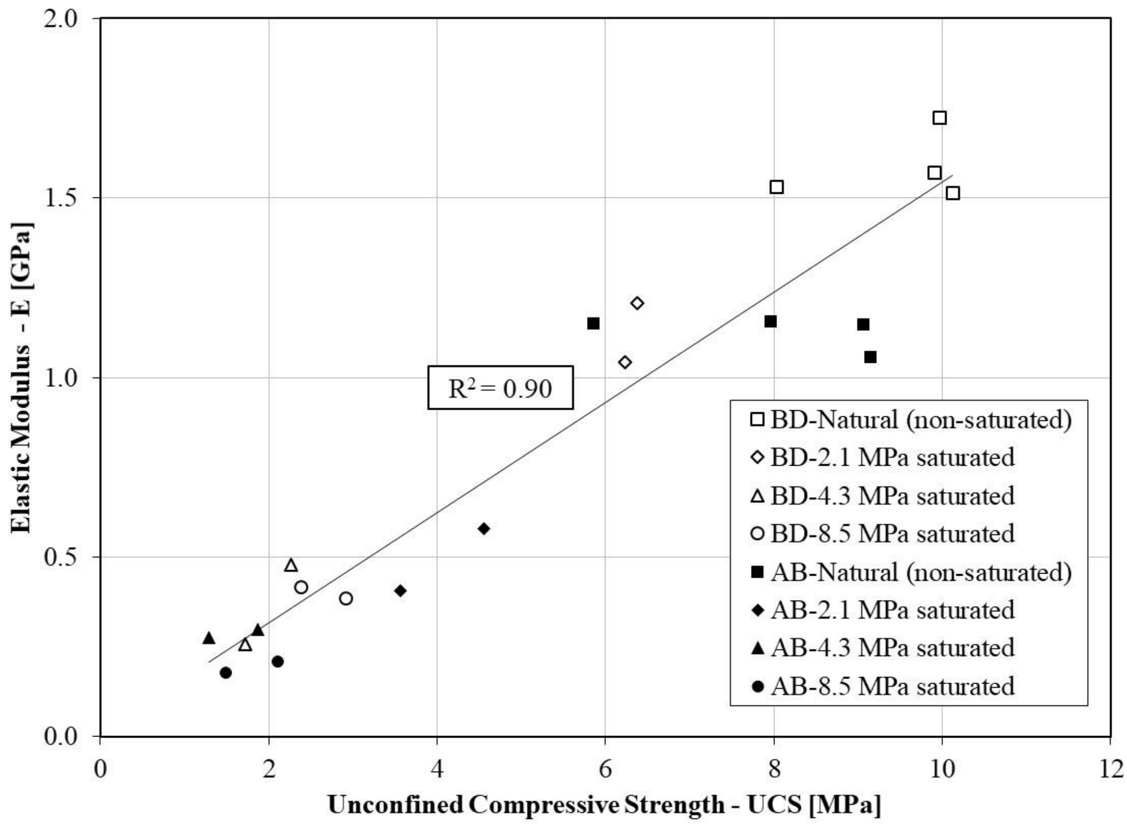

Fig. 6. Uniaxial compressive strengths vs elastic moduli of natural (non-saturated) and CO_2-saturated coal specimens.

Average values of reduction of measured parameters of both coals versus the gas pressure are plotted in Fig. 7. A deviation of parameters between the coals saturated at 2.1 MPa can be observed. In particular, BD samples experienced 29% average reduction in elastic modulus and 34% average reduction in compressive strength. AB samples showed 49% and 56% average reductions in compressive strength and elastic modulus, respectively. As mentioned earlier, Perera et al. (2011) and Ranathunga et al. (2016a) conducted a deformation analysis on lignite coals saturated with CO_2 at 2.1 MPa and 2.0 pressure, respectively. Hence, by comparing the reduction values of samples saturated with CO_2 at 2.1 MPa in this study (i.e. reductions between 29% and 56%) to the reduction values reported in the literature by Perera et al. (2011), i.e. 7-19%, and Ranathunga et al. (2016a), i.e. 6-16%, it can be concluded that saturation of anthracite coal with CO_2 has a more detrimental effect on the measured parameters than of lignite coal subjected to CO_2 at the same pressure. Also, the reduction of parameters measured in this study at 8.5 MPa (72-83%) is greater than the one reported by Ranathunga et al. (2016a) for lignite (40-58%) saturated at 8 MPa, however comparable to the result reported by Perera et al. (2013) for bituminous coal (71-79%) saturated at 8 MPa.

By observing the shape of the curve presented in Fig. 7, it can be inferred that the calculated reductions in measured parameters increase gradually up to 80% at 4.3 MPa and then reach a plateau. Such findings for high rank anthracitic coals are different from the work of Perera et al. (2013) and Ranathunga et al. (2016a) who reported that bituminous and lignite coals exhibit a sudden reduction in mechanical parameters during the transition from subcritical CO_2 at 6 MPa to supercritical CO_2 at 8 MPa.

This might be related to the difference in sorption behaviour of low ranks coals compared to high ranks coals. Siemons and Busch (2007) and Gensterblum et al. (2010) have shown that low rank coals exhibit half of their sorption at higher pressures (e.g. 3.77 MPa) while high rank coals show the opposite behaviour, i.e. half of the sorption is reached at lower pressures (e.g. 0.96 MPa). Similar observation was made by Zagorščak (2017) where BD and AB cores exhibited half of their maximum sorption at pressures lower than 1 MPa. Consequently, it can be expected that majority of structural re-arrangement and its effect on coal strength and elastic modulus occurred in the subcritical region, up to 4.3 MPa in this case, whereas no significant change has been observed with further increase in gas pressure.

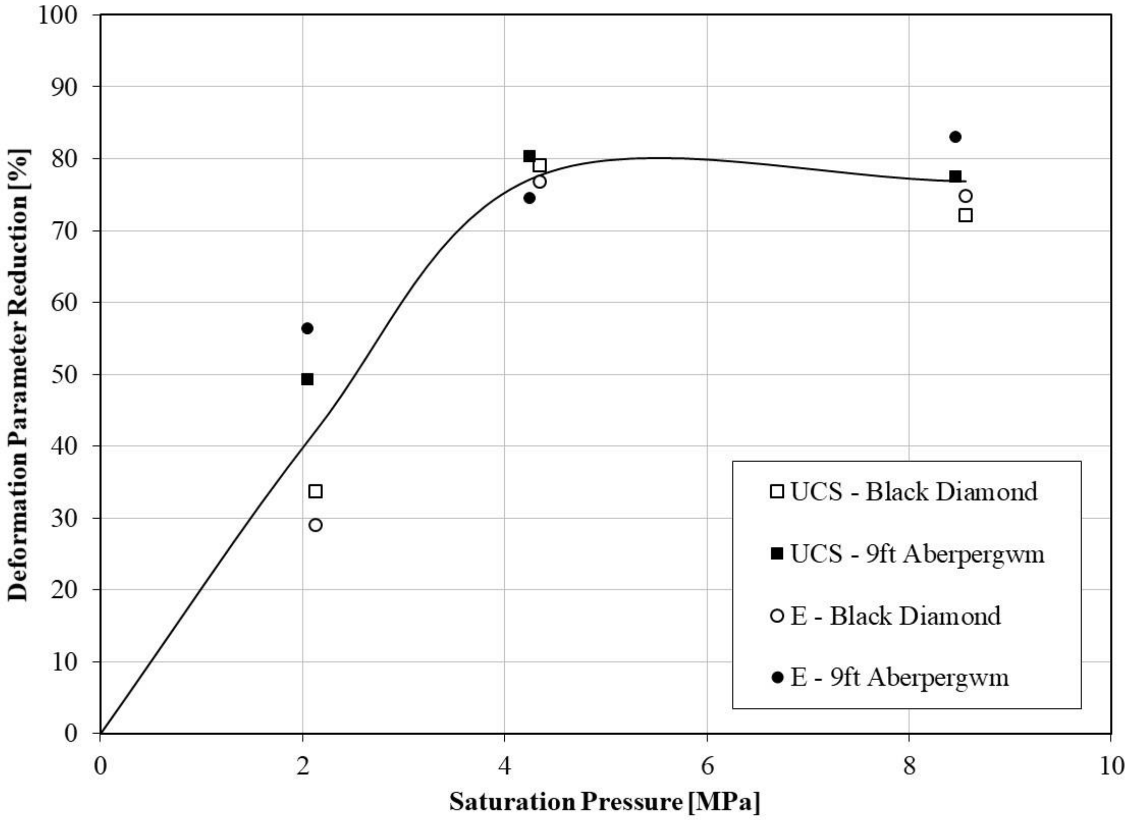

Fig. 7. Reduction of deformation parameters with an increase in CO_2 saturation pressure.

It has been previously suggested that coal samples subjected to sorbing gas are weakened through reduction of effective stress and the internal gas energy release (Wang et al., 2013). Hence, in order to get further insight into the effect of CO_2 sorption and try to distinguish between the effect of effective stress and the alteration of coal structure induced by CO_2 sorption on the strength reduction, both the effective and the residual unconfined compressive strengths versus the saturation pressures are presented in Fig. 8. The effective unconfined compressive strength values were calculated by subtracting the saturation pressures from the unconfined compressive strength determined on samples not saturated with CO_2. It should be noted that during the uniaxial compressive testing, the gas pressure in the samples was not measured. However, it was assumed that due to slow sorption of the CO_2, especially in its subcritical state, on the microporous matrix of the high rank coals and testing the samples within one hour of being removed from the saturation chamber (Zagorščak, 2017), the pressure inside each coal sample remained close to the saturation pressure. Hence, the saturation pressure, which represents the maximum limit to the potential pressure in the fractures, was taken for calculation of the effective unconfined compressive strength. The residual unconfined compressive strength values represent the average strength values measured on samples saturated with CO_2 at different pressures.

Since compressive strengths should index with effective stresses (Wang et al., 2013), Fig. 8 suggests that at sorption pressures of 2.1 MPa and 4.3 MPa, the compressive strengths are reduced by more than the applied saturation pressure. This implies that potentially chemical or other influence of CO_2 sorption, such as reduction of breakdown pressures, is reducing the strength as it is known that carbon dioxide dissolves in coal enabling physical structure rearrangements (e.g. Larsen, 2004). In particular, residual strengths are up to 32% and 62% lower than the effective compressive strengths for samples saturated at 2.1 MPa and 4.3 MPa, respectively. Hence, the effect of CO_2 sorption on the structural rearrangement increases with saturation pressure within the subcritical region. However, further inspection of Fig. 8 shows that residual strengths of coals saturated at 8.5 MPa are higher than effective compressive strengths. Therefore, it can be inferred that the maximum alteration of the coal structure due to CO_2 adsorption was achieved at 4.3 MPa and that increasing the saturation pressure from subcritical CO_2 to its supercritical state had negligible impact on further reduction of strength. As previously mentioned, the results are contrary to the findings suggested in the literature that CO_2 phase transition from subcritical to supercritical state results in 40% and 46 % greater strength reduction for bituminous and brown coals, respectively (e.g. Perera et al. 2013; Ranathunga et al., 2016a).

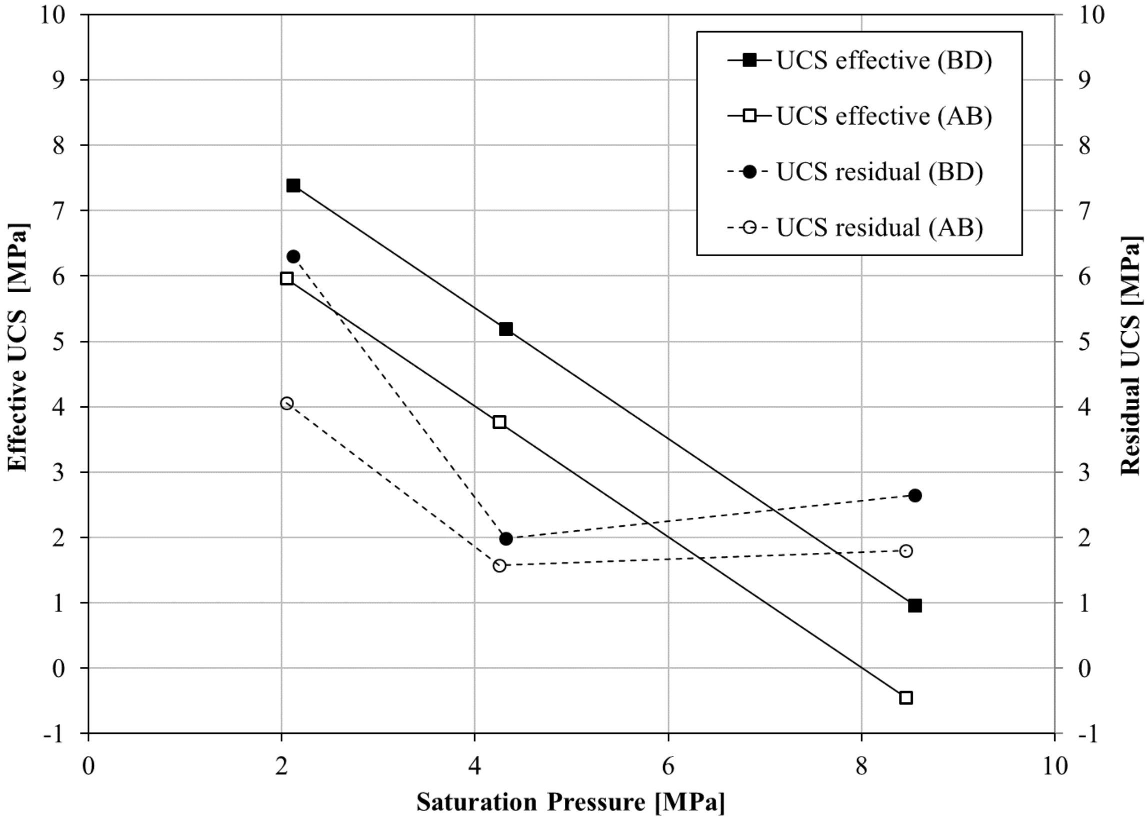

Fig. 8. Comparison between the Effective UCS and Residual UCS with respect to CO_2 saturation pressure.

3.1. Parametrisation of changes in UCS and E

The observed reductions in elastic modulus and unconfined compressive strength values are quantified by fitting a simple model to the experimental results and obtaining the fitting parameters. Since the change in measured parameters is caused by gas sorption, such change can be mathematically related to gas pressure (Masoudian et al., 2014).

Following the approach that the elastic modulus reduction is most commonly modelled using a Langmuir (1918) equation, ΔE can be written as (Masoudian et al., 2014):

$$\Delta E = \Delta E_{max} \frac{P}{P_E + P} \quad (3)$$

where ΔE_{max} is the maximum reduction in elastic modulus (Langmuir parameter), P is the gas pressure (MPa) and P_E is the Langmuir pressure (MPa) of elastic modulus reduction.

Similarly, ΔUCS can be written as (Masoudian et al., 2014):

$$\Delta UCS \ = \Delta UCS_{max} \frac{P}{P_{UCS}+P} \quad (4)$$

where ΔUCS_{max} is the maximum reduction in strength (Langmuir parameter) and P_{UCS} is the Langmuir pressure (MPa) of unconfined compressive strength reduction.

The fitting of the Langmuir curve to the experimental data was conducted using the sum of the squared differences with a target function which was minimized with respect to the Langmuir parameters using the Excel solver function.

Fig. 9 and Fig. 10 present the curves fitted to the experimental data of unconfined compressive strength and elastic modulus reductions of both samples as a function of CO_2 pressure, respectively. The parameters obtained using the fitting approach related to the reduction of deformation parameters of both coals are shown in Table 5. The unconfined compressive strength and elastic modulus of CO_2 saturated AB coal experience half of their maximum reduction at 1.69 MPa and 1.53 MPa gas pressures, respectively. In comparison, BD experienced half of the maximum reduction of unconfined compressive strength and elastic modulus at 2.53 MPa and 2.74 MPa, respectively.

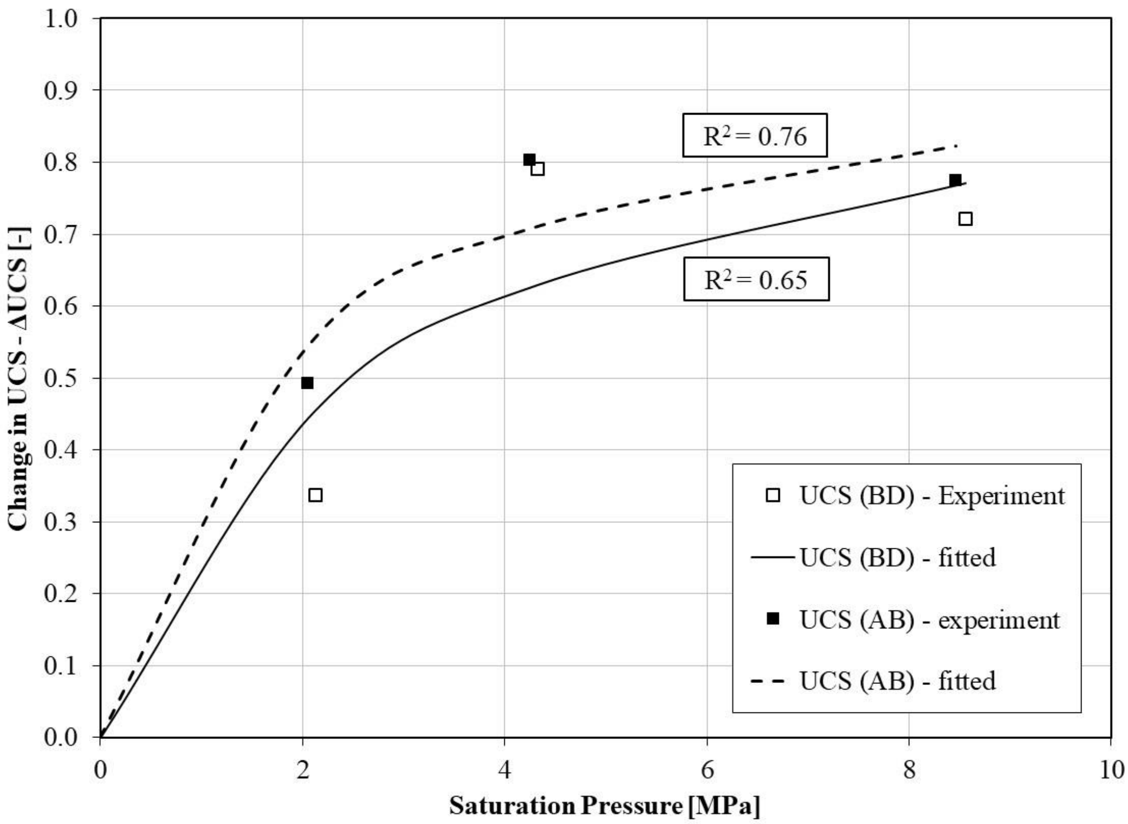

Fig. 9. The unconfined compressive strength reduction isotherms fitted to the calculated unconfined compressive strength reduction values of BD and AB coals.

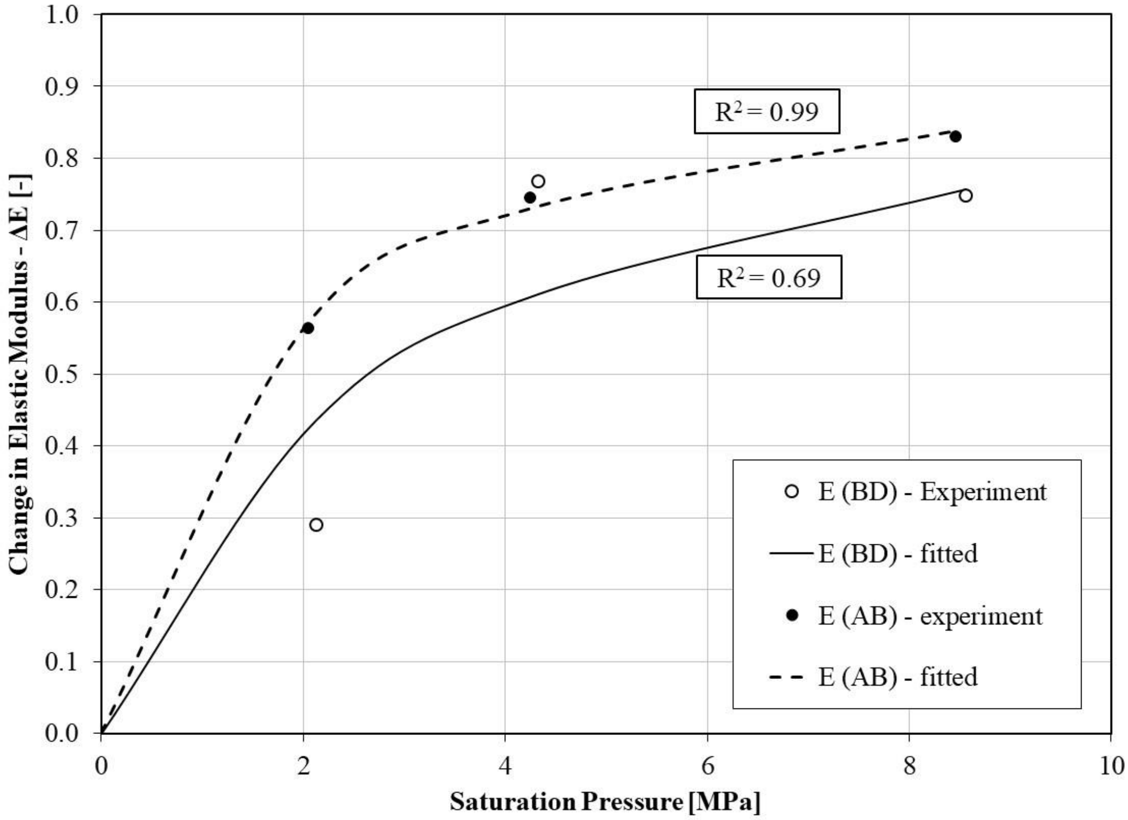

Fig. 10. The elastic modulus reduction isotherms fitted to the calculated elastic modulus reduction values of BD and AB coals.

Table 5.
Fitted parameters of the proposed model for reduction of unconfined compressive strength and elastic modulus of BD and AB coals.

Deformation parameter	**Fitted (Langmuir) parameters**	
	P_{UCS} (MPa), P_E (MPa)	**UCS_{max} (-), E_{max} (-)**
Black Diamond		
Unconfined compressive strength	2.53	1.0
Elastic modulus	2.74	1.0
9ft Aberpergwm		
Unconfined compressive strength	1.69	0.98
Elastic modulus	1.53	0.99

3.2. Failure patterns

To visualize the effect of CO_2 saturation on failure mechanism of the coals considered in this study, photographs were taken before and after the failure of both natural and CO_2 saturated specimens. The photographs containing natural (non-saturated) samples and samples saturated at 2.1 MPa, 4.3 MPa and 8.5 MPa are shown in Fig. 11, 12, 13 and 14, respectively.

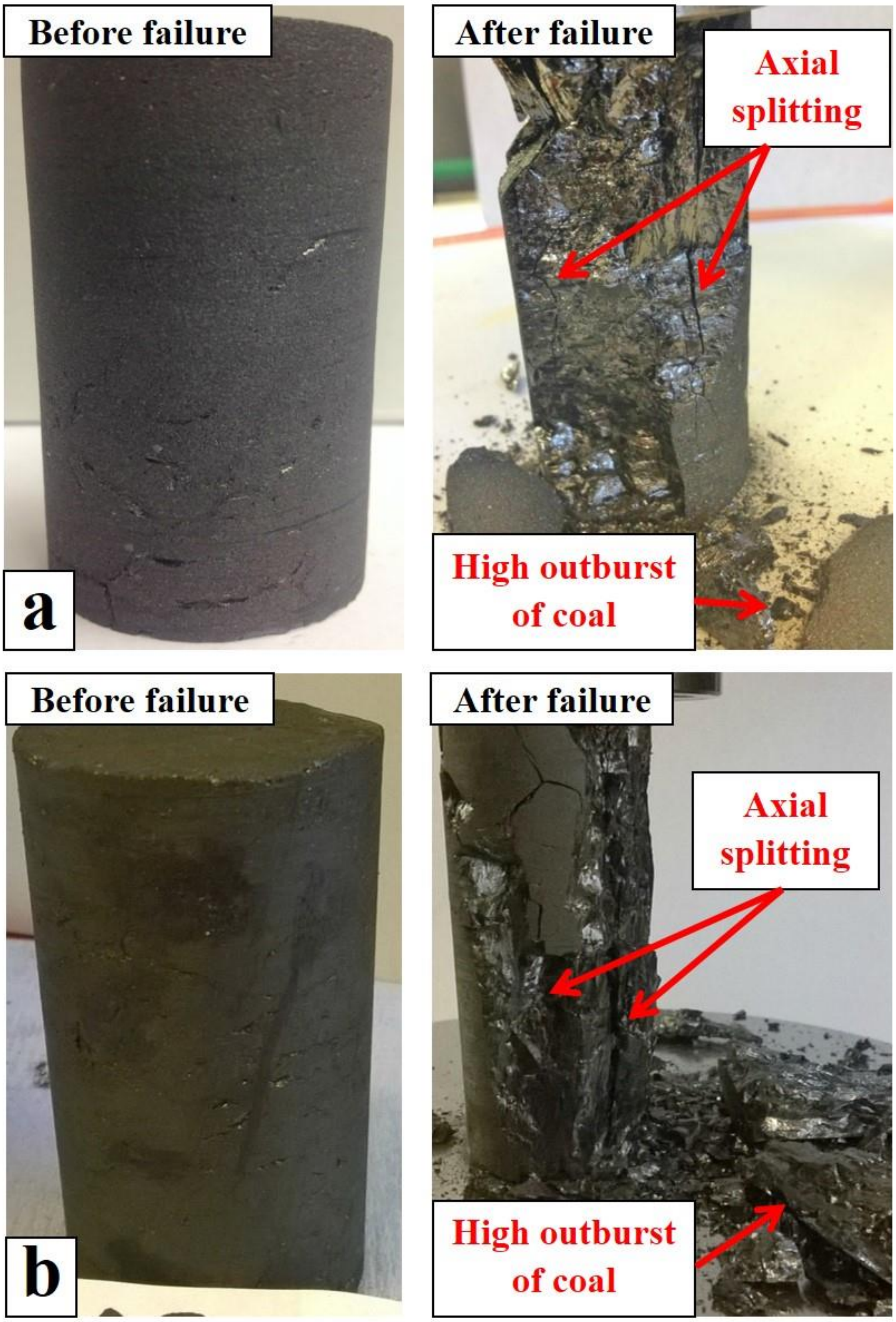

Fig. 11. Failure patterns of non-saturated coal samples; A) Black Diamond, B) 9ft Aberpergwm.

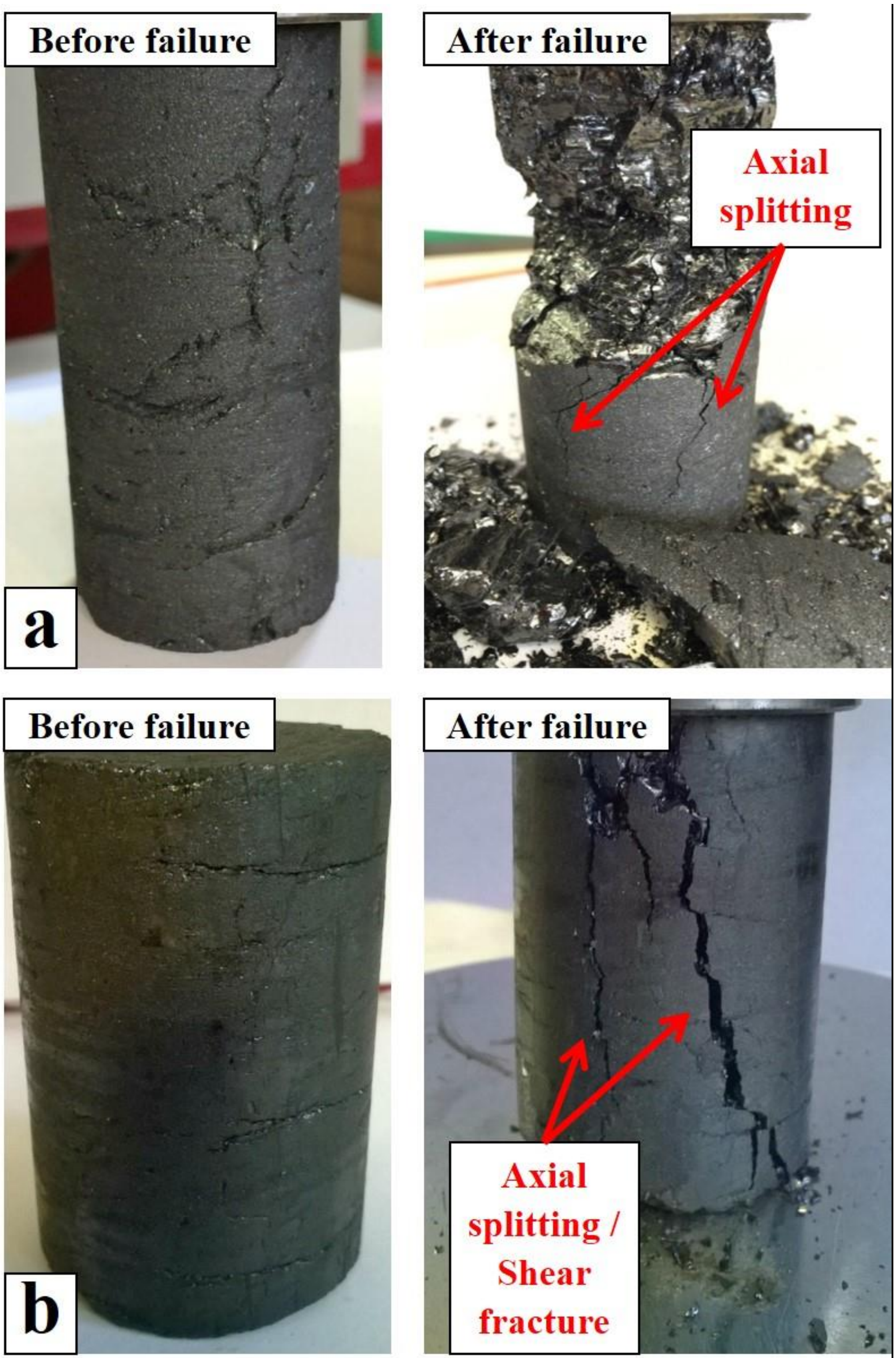

Fig. 12. Failure patterns of samples saturated with CO_2 at 2.1 MPa; A) Black Diamond, B) 9ft Aberpergwm.

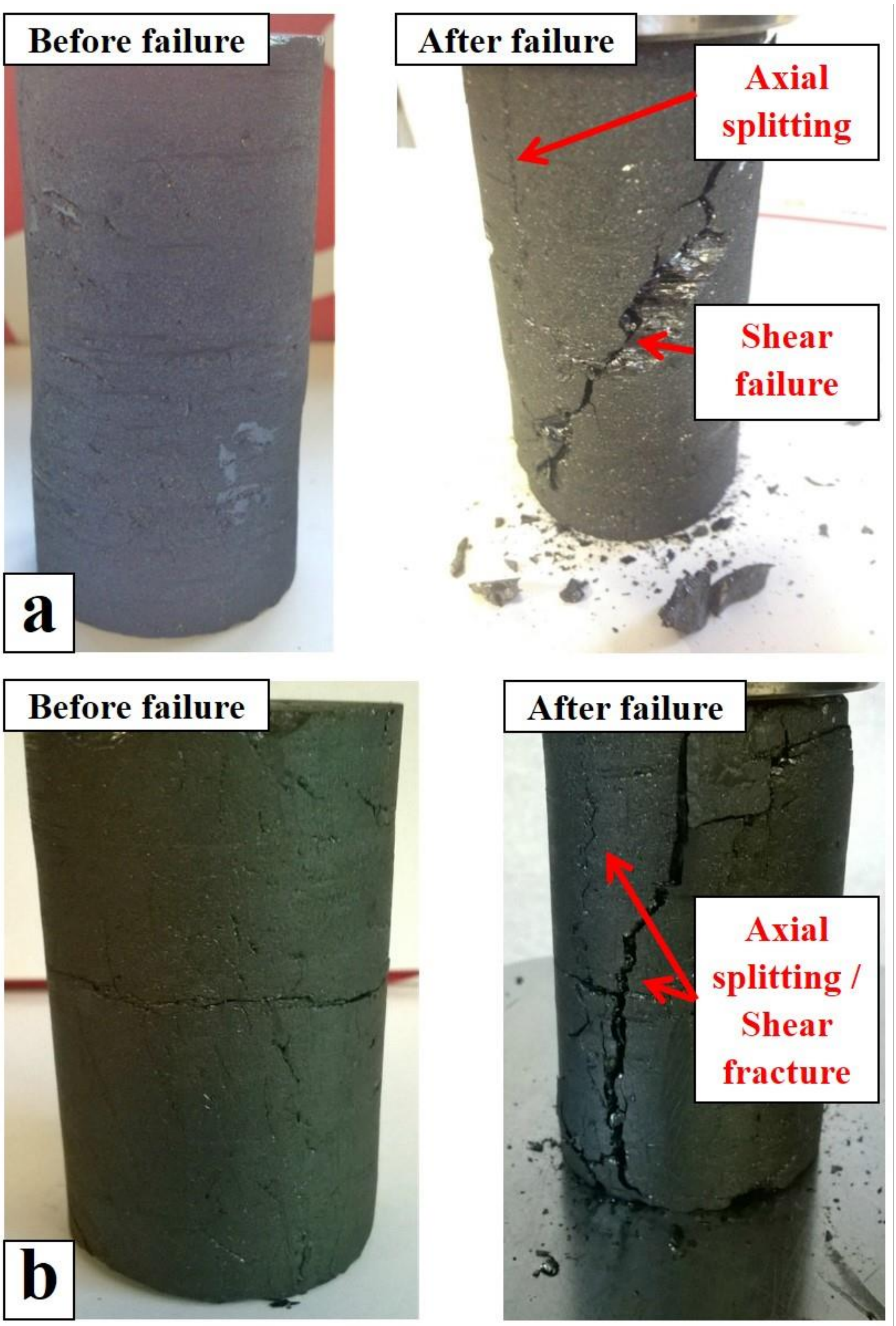

Fig. 13. Failure patterns of samples saturated with CO_2 at 4.3 MPa; A) Black Diamond, B) 9ft Aberpergwm.

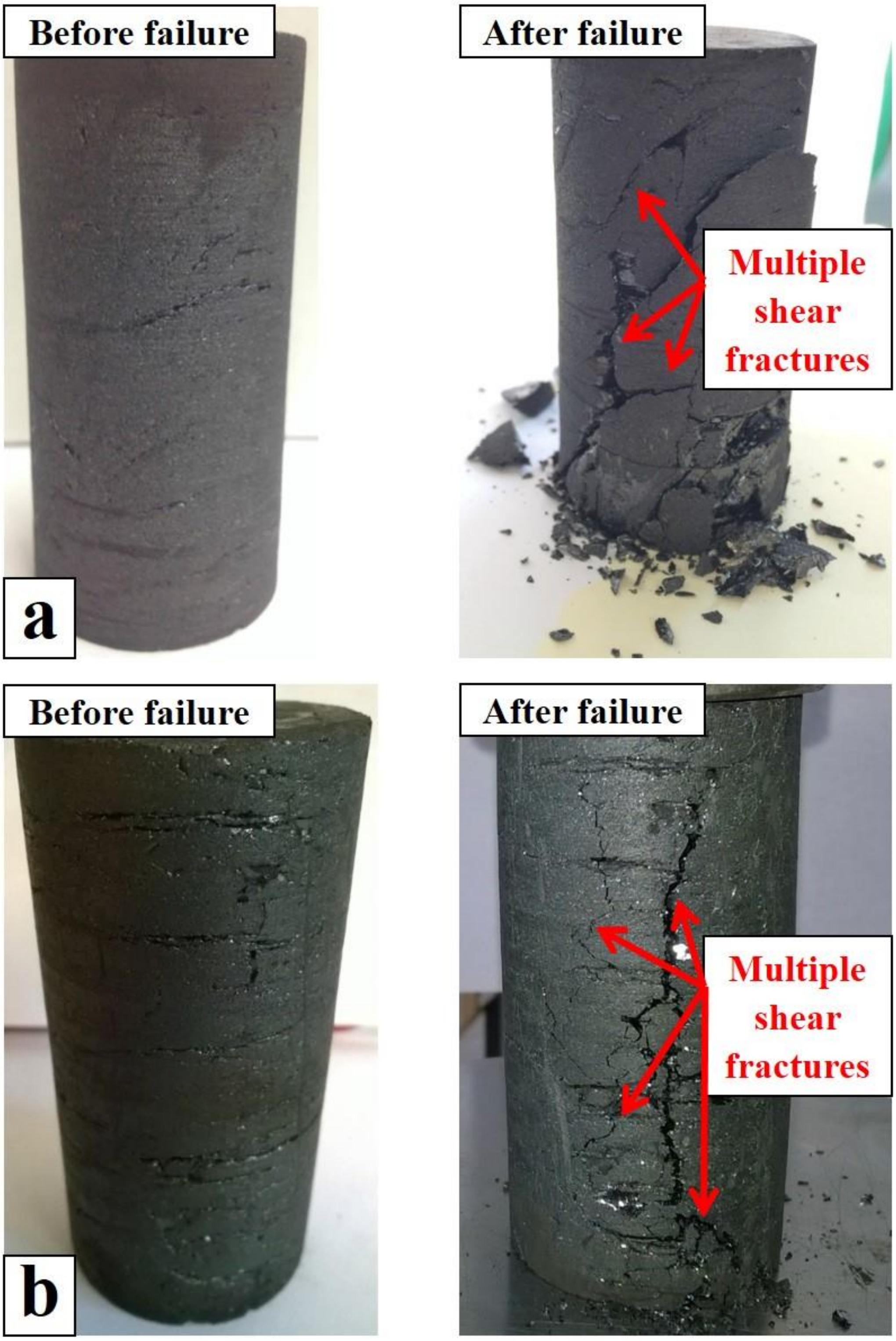

Fig. 14. Failure patterns of samples saturated with CO_2 at 8.5 MPa; A) Black Diamond, B) 9ft Aberpergwm.

Non-saturated coal samples failed predominantly through axial splitting where a number of axial cracks propagated along the entire length of the specimens (Fig. 11). Such splitting occurred with rapid and unstable crack initiation and propagation, common for brittle materials, outbursting the samples into pieces.

Samples saturated with CO_2 at 2.1 MPa showed similar behaviour to those of non-saturated samples (Fig. 12). However, a set of non-longitudinal fractures was also visible, especially on the AB sample. Predominant shear failure occurred in samples saturated at 4.3 MPa of CO_2 (Fig. 13). In addition, a set of axial fractures was visible for both samples suggesting that the overall failure could be a combination of fracture propagation in axial and non-axial directions. For coals saturated in supercritical CO_2, i.e. at 8.5 MPa, multiple shear fractures orientated in different directions occurred with negligible material outburst during failure (Fig. 14).

Interestingly, both BD and AB samples showed comparable behaviour in terms of failure patterns. The only distinction is for specimens saturated at 2.1 MPa where BD exhibited higher outburst of the material than the AB coal showing predominantly axial splitting within the BD coal. This is in accordance with the strength parameter reduction (Fig. 7) where it is shown that AB samples saturated at 2.1 MPa lost more than half of their original strength while BD samples lost a third of their original strength. Consequently, higher residual strength of the BD coal could have resulted in a behaviour more similar to the natural, non-saturated samples.

Overall, by comparing failure types of non-saturated and CO_2 saturated specimens, a distinction can be observed. While former ones show predominantly axial splitting, the latter ones fail through a visible shear plane and existing fractures weakened by the CO_2 sorption. In unconfined compressive tests, irregular longitudinal splitting is the most common failure mechanism observed leading to an abrupt failure (Jaeger et al. 2007). Where the rock is fully ductile, a network of shear fractures will develop accompanied by plastic deformation of individual grains (Jaeger et al. 2007).

3.3. Post-failure sieve analysis

To assess the impact of CO_2 sorption on coal structure over the range of pressures used in this study, a post-failure sieve analysis of ten BD coal specimens was conducted. Fig. 15 shows coal particles as a result of a failure of both non-saturated and CO_2 saturated BD samples under axial compression. The failure of the non-saturated sample resulted in a large coal lump accompanied by a number of smaller particles. Conversely, CO_2 saturated samples show more gradual distribution of the coal particles.

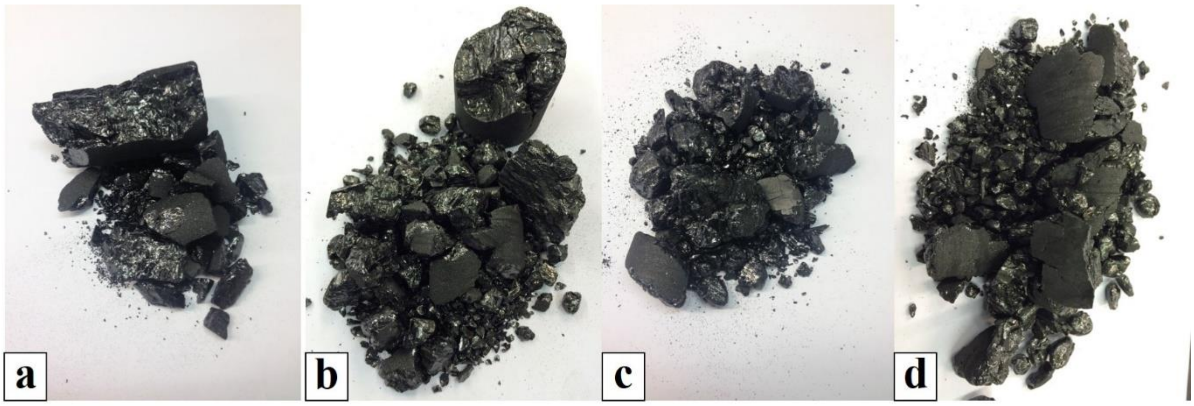

Fig. 15. Black Diamond coal post-failure particles; (a) natural (non-saturated) sample, (b) 2.1 MPa saturated sample; (c) 4.3 MPa saturated sample, (d) 8.5 MPa saturated sample.

Based on the results of the sieve analysis of ten BD specimens, the average percentage of particles passing through a certain sieve for natural and CO_2 saturated specimens was calculated. Comparison of the obtained average values with respect to sieve size is presented in Fig. 16.

Specimens saturated with CO_2 show higher percentage of particles passing through sieves than non-saturated specimens. On average, 7%, 15%, 28% and 30% of the total coal mass of non-saturated, 2.1 MPa saturated, 4.3 MPa saturated and 8.5 MPa saturated coal specimens passed through the largest sieve size of 6.3 mm, respectively. Such results confirm the previous assumption by Wang et al. (2011) that CO_2 saturated coals would result in smaller particles after the failure than the non-saturated specimens indirectly suggesting the micro-fracturing of the coal caused by CO_2 sorption. Additionally, it can be inferred from Fig. 16 that the percentage of particles passing through sieves depends on saturation pressure.

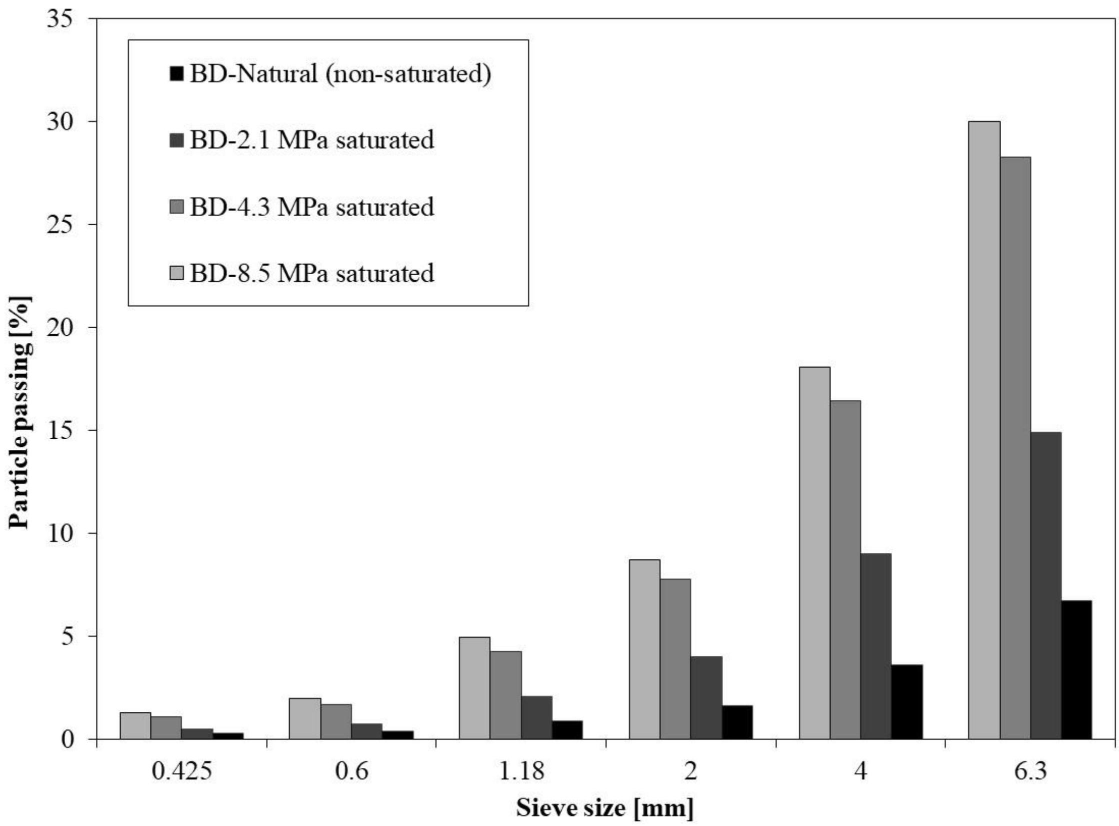

Fig. 16. Comparison of the post-failure particle size distribution of natural (non-saturated) and CO_2 saturated Black Diamond samples.

In order to assess the difference in percentages of particles passing through each sieve between the non-saturated and CO_2 saturated samples, Fig. 17 shows the passing ratio versus the gas saturation pressure for each sieve. Passing ratio is calculated as the average percentage of particles passing through an individual sieve for CO_2 saturated samples divided by the average percentage of particles passing for natural (non-saturated) coal specimens.

Fig. 17 shows that for specimens saturated at 2.1 MPa, there are 1.7 to 2.5 more particles passing through the sieves compared to non-saturated specimens. For specimens saturated at 4.3 MPa and 8.5 MPa, the amount of particles passing through all the sieves compared to non-saturated specimens is 3.9-4.9 and 4.5-5.6 times higher, respectively. Hence, as the saturation pressure increases, the passing ratio steeply increases up to 4.3 MPa and then shows a more gradual further increase with gas pressure.

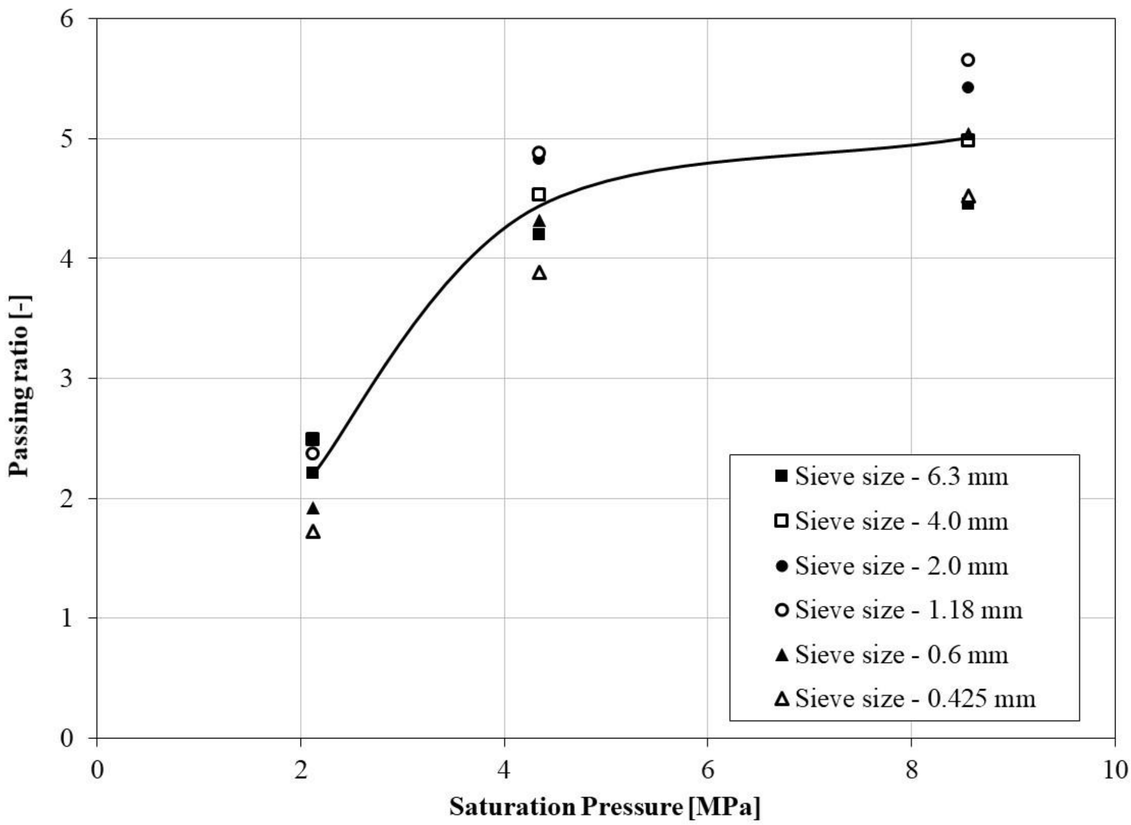

Fig. 17. Passing ratio versus the saturation pressure for particles passing through sieves of different sizes.

4. Discussion and Conclusions

The main aim of this study was to investigate the influence of sub- and supercritical CO_2 sorption on elastic deformation and failure of unconfined coal specimens subject to axial load. Two high rank coals collected from different locations of the South Wales Coalfield and from depths of 150 m (Black Diamond coal) and 550 m (Aberpergwm 9ft coal) were considered and in total, 20 samples were tested.

Based on the results of this study, unconfined compressive strengths and elastic moduli exhibit a linear relationship demonstrating that any loss in the elastic modulus is accompanied by the corresponding loss in the compressive strength of high rank coals.

The results also show that samples of both coals experience maximum reduction in elastic modulus and strength at 4.3 MPa, i.e. between 75% and 80%, where CO_2 is in the gaseous state. However, additional increase in CO_2 pressure to its supercritical state at 8.5 MPa had negligible effect on further reduction in measured parameters which was measured to be between 72% and 83%. Hence, this leads to the conclusion that the reduction of elastic modulus and compressive strength of high rank coals is related to their sorptive behaviour. In other words, by achieving more than half of their maximum sorption capacity in the low pressure subcritical region, the corresponding structural rearrangement and consequent reduction in measured geomechanical parameters of high rank coals occurs in the same pressure region. This has been further confirmed by accommodating the effect of effective stress which suggested that chemical weakening of coal through its structural rearrangement occurs in the subcritical region and that there is a negligible further weakening effect due to the presence of supercritical CO_2 which is contrary to the findings previously reported in the literature for lignite and bituminous coals.

Although BD coal showed higher absolute values of unconfined compressive strengths and elastic moduli than the AB coal, the reduction percentage of deformation parameters of both samples is similar, especially at 4.3 MPa and 8.5 MPa saturation pressures. Hence, despite both anthracite coals considered in this study being from different locations and depths of the South Wales Coalfield, similar trends obtained on the samples of both coals suggest that geomechanical property alterations are rank related.

Visual inspection of the failure patterns showed that non-saturated specimens failed predominantly through axial splitting with high outburst of the material during compression, while the failure of the cores saturated with CO_2 occurred through a combination of shear fractures oriented in different directions with negligible material outburst common for ductile materials. Possible formation of micro fractures in the CO_2 saturated samples, previously suggested in the literature, was further confirmed by the results of the post-failure sieve analysis. The results showed that on average, only 7% of non-saturated particles passed through 6.3 mm sieve, while 2.1 MPa saturated, 4.3 MPa and 8.5 MPa saturated coals showed 15%, 28% and 30% of particles passing through the same sieve, respectively. Under those circumstances, it can be concluded due to the fact that CO_2 treated samples disintegrated on smaller particles than specimens without any CO_2 saturation after the failure, geomechanical property changes are a result of the weakened coal structure through the enhancement of the existing and inducement of new fractures.

Overall, this study demonstrated the weakening effect of CO_2 on high-rank anthracitic coals making them more ductile and less resistive to deformation under applied stress. Presented observations imply that the reduction of the coal deformation properties due to CO_2 sorption could contribute to the overall performance of a coal seam subject to CO_2 sequestration. On one hand, coal weakening could have a potentially negative impact on the structural integrity of the CO_2 storage reservoir which could be eliminated by targeting coal seams with structurally sound overburden.

On the other hand, enhancement of existing fractures and creation of new ones could be a positive feature from the CO_2 injection standpoint as newly formed fractures could offer additional pathways for CO_2 flow and increase the amount of CO_2 injected in seams by offsetting the impact of coal swelling on CO_2 injectivity. Furthermore, reduction in elastic modulus of the target coals would result in increasing the fracture apertures under high pressure gas flow, again enabling easier access for the CO_2 molecules to the sorption sites. Based on the abovementioned, it can be implied that high rank coals could offer a good prospect of storing CO_2. Hence, future work will focus to enhance the current understanding of how the changes in deformation properties induced by CO_2 sorption affect the coal's transport and storage properties.

According to the author's knowledge, this is the first experimental analysis of anthracite coal's behaviour as well as the behaviour of South Wales coals dealing with the change in deformation properties of coals subject to sub- and supercritical CO_2 pressures up to 8.5 MPa.

5. Acknowledgements

This work was carried out as a part of SEREN and FLEXIS Projects. Both projects have been part-funded by the European Regional Development Fund through the Welsh Government. The financial support, for the first author, is gratefully acknowledged. The authors wish to express their appreciation to EnergyBuild Ltd, Walter Energy Inc. and Celtic Energy Ltd for providing coal blocks to conduct this research.

6. References

ASTM Standards, 2012. *ASTM D2013. Standard practice of preparing coal samples for analysis. Vol. 05.06.* West Conshohocken, PA: ASTM International.

ASTM Standards, 2014. *ASTM D7012. Standard Test Methods for Compressive Strength and Elastic Moduli of Intact Rock Core Specimens under Varying States of Stress and Temperatures. Vol. 04.09.* West Conshohocken, PA: ASTM International.

ASTM Standards, 2015. *ASTM D388. Standard Classification of Coals by Rank. Vol. 05.06.* West Conshohocken, PA: ASTM International.

ASTM Standards, 2015. *ASTM D3302/D3302M. Standard Test Method for Total Moisture in Coal. Vol. 05.06.* West Conshohocken, PA: ASTM International.

British Standards Institution, 1990. *BS 1377-2:1990. Methods of test for soils for civil engineering purposes. Clasification tests.* Milton Keynes: BSI.

British Standards Institution, 1996. *BS 1016-106.1.1:1996. Methods for analysis and testing of coal and coke. Ultimate analysis of coal and coke. Determination of carbon and hydrogen content, high temperature combustion method.* Milton Keynes: BSI.

British Standards Institution, 1996. *BS 1016-106.4.2:1996. Methods for analysis and testing of coal and coke. Ultimate analysis of coal and coke. Determination of total sulfur content, high temperature combustion method*. Milton Keynes: BSI.

British Standards Institution, 1998. *BS 1016-104.3:1998. Methods for analysis and testing of coal and coke. Proximate analysis, determination of volatile matter content.* Milton Keynes: BSI.

British Standards Institution, 1998. *BS 1016-104.4:1998. Methods for analysis and testing of coal and coke. Proximate analysis, determination of ash.* Milton Keynes: BSI.

British Standards Institution, 1999. *BS 1016-104.1:1999. Methods for analysing and testing of coal and coke. Proximate analysis, determination of moisture content of the general analysis tests sample.* Milton Keynes: BSI.

Busch, A. and Gensterblum, Y. 2011. CBM and CO2-ECBM related sorption processes in coal: A review. *International Journal of Coal Geology*, 87(2), pp. 49-71.

Gathitu, B.B., Chen, W.Y. and McClure, M. 2009. Effects of Coal Interaction with Supercritical CO_2: Physical Structure. *Industrial & Engineering Chemistry Research*, 48(10), pp. 5024-5034.

Gensterblum, Y. 2013. *CBM and CO_2-ECBM related sorption processes in coal.* Ph.D. Thesis, RWTH Aachen University, Germany.

Gensterblum, Y., van Hemert, P., Billemont, P., Battistutta, E., Busch, A., Krooss, B.M., De Weireld, G. and Wolf, K.H.A.A. 2010. European inter-laboratory comparison of high pressure CO_2 sorption isotherms II: Natural coals. *International Journal of Coal Geology.* 84(2), pp. 115-124.

Hol, S., Spiers, C.J. and Peach, C.J. 2012. Microfracturing of coal due to interaction with CO_2 under unconfined conditions. *Fuel*, 97, pp. 569-584.

Hol, S., Gensterblum, Y. and Massarotto, P. 2014. Sorption and changes in bulk modulus of coal – experimental evidence and governing mechanisms for CBM and ECBM applications. *International Journal of Coal Geology*, 128-129, pp. 119-133.

Jaeger, J.C., Cook, N.G.W. and Zimmerman, R.W. 2007. *Fundamentals of Rock Mechanics*, 4th Edition, Blackwell Publishing.

Jones, N.S., Holloway, S., Smith, N.J.P., Browne, M.A.E., Creedy, D.P., Garner, K. and Durucan, S. 2004. *UK Coal Resource for New Exploitation Technologies.* DTI Report No. COAL R271, DTI/Pub URN 04/1879. DTI Cleaner Coal Technology Transfer Programme, Harwell.

Karacan, C.Ö. 2007. Swelling-induced volumetric strains internal to a stressed coal associated with CO_2 sorption. *International Journal of Coal Geology*, 72(3-4), pp. 209-220.

Langmuir, I. 1918. The adsorption of gases on plane surfaces of glass, mica and platinum. *Journal of the American Chemical Society*, 40(9), pp. 1361-1403.

Larsen, J.W. 2004. The effects of dissolved CO_2 on coal structure and properties. *International Journal of Coal Geology*, 57, pp. 63-70.

Li, D., Liu, Q., Weniger, P., Gensterblum, Y., Busch, A. and Krooss, B.M. 2010. High-pressure sorption isotherms and sorption kinetics of CH_4 and CO_2 on coals. *Fuel*, 89(3), pp. 569-580.

Liu, C.J., Wang, G.X., Sang, S.X. and Rudolph, V. 2010. Changes in pore structure of anthracite coal associated with CO_2 sequestration process. *Fuel*, 89(10), pp. 2665-2672.

Liu, C.J., Wang, G.X., Sang, S.X., Gilani, W. and Rudolph V. 2015. Fractal analysis in pore structure of coal under conditions of CO_2 sequestration process. *Fuel*, 139, pp. 125-132.

Masoudian, M.S., Airey, D.W. and El-Zein, A. 2014. Experimental investigations on the effect of CO_2 on mechanics of coal. *International Journal of Coal Geology*, 128-129, pp. 12-23.

Perera, M.S.A., Ranjith, P.G. and Peter, M. 2011. Effects of saturation medium and pressure on strength parameters of Latrobe Valley brown coal: Carbon dioxide, water and nitrogen saturations. *Energy*, 36(12), pp. 6941-6947.

Perera, M.S.A., Ranjith, P.G. and Viete, D.R. 2013. Effects of gaseous and super-critical carbon dioxide saturation on the mechanical properties of bituminous coal from the Southern Sydney Basin. *Applied Energy*, 110, pp. 73-81.

Ranathunga, A.S., Perera, M.S.A., Ranjith, P.G. and Bui, H. 2016a. Super-critical CO_2 saturation-induced property alterations in low rank coal: An experimental study. *The Journal of Supercritical Fluids*, 109, pp. 134-140.

Ranathunga, A.S., Perera, M.S.A. and Ranjith P.G. 2016b. Influence of CO2 adsorption on the strength and elastic modulus of low rank Australian coal under confining pressure. *International Journal of Coal Geology*, 167, pp. 148-156.

Ranjith, P.G. and Perera, M.S.A. 2012. Effects of cleat performance on strength reduction of coal in CO_2 sequestration. *Energy*, 45(1), pp. 1069-1075.

Siemons, N. and Busch, A. 2007. Measurement and interpretation of supercritical CO_2 sorption on various coals. *International Journal of Coal Geology*, 69(4), pp. 229-242.

Viete, D.R. and Ranjith, P.G. 2006. The effect of CO_2 on the geomechanical and permeability behaviour of brown coal: Implications for coal seam CO_2 sequestration. *International Journal of Coal Geology*, 66, pp. 201-216.

Vishal, V., Ranjith, P.G. and Singh, T.N. 2015. An experimental investigation on behaviour of coal under fluid saturation, using acoustic emission. *Journal of Natural Gas Science and Engineering.* 22, pp. 428-436.

Wang, S., Elsworth, D. and Liu, J. 2011. Permeability evolution in fracture coal: the roles of fracture geometry and water-content. *International Journal of Coal Geology*, 87(1), pp. 13-25.

Wang, S., Elsworth, D. and Liu, J. 2013. Mechanical Behavior of Methane Infiltrated Coal: the Roles of Gas Desorption, Stress Level and Loading Rate. *Rock Mechanics and Rock Engineering*, 46, pp. 945-958.

White, C.M., Smith, D.H., Jones, K.L., Goodman, A.L., Jikich, S.A., Lacount, R.B., Dubose, S.B., Ozdemir, E., Morsi, B., Schroeder, K.T. 2005. Sequestration of Carbon Dioxide in Coal with Enhanced Coalbed Methane Recovery – A Review. *Energy&Fuels*, 19 (3), 659-724.

Zagorščak, R. 2017. *An Investigation of Coupled Processes in Coal in Response to High Pressure Gas Injection.* Ph.D. Thesis, Cardiff University, Wales, UK.